Synchrotron Radiation News

ISSN: 0894-0886 (Print) 1931-7344 (Online) Journal homepage: http://www.tandfonline.com/loi/gsrn20

Advancements and Application of Microsecond Synchrotron X-ray Footprinting at the Advanced Light Source

Sayan Gupta, Rich Celestre, Jun Feng & Corie Ralston

To cite this article: Sayan Gupta, Rich Celestre, Jun Feng & Corie Ralston (2016) Advancements and Application of Microsecond Synchrotron X-ray Footprinting at the Advanced Light Source, Synchrotron Radiation News, 29:1, 39-44, DOI: 10.1080/08940886.2016.1124684

To link to this article: http://dx.doi.org/10.1080/08940886.2016.1124684

Published online: 01 Feb 2016.

Advancements and Application of Microsecond Synchrotron X-ray Footprinting at the Advanced Light Source

SAYAN GUPTA,[1] RICH CELESTRE,[2] JUN FENG,[2] AND CORIE RALSTON[1]

[1]*Molecular Biophysics and Integrated Bioimaging, Lawrence Berkeley National Laboratory, Berkeley, California, USA*

[2]*Experimental Systems, Advanced Light Source, Lawrence Berkeley National Laboratory, Berkeley, California, USA*

Introduction

The method of synchrotron X-ray protein footprinting (XF-MS) is used to determine protein conformational changes, folding, protein-protein and protein-ligand interactions, providing information which is often difficult to obtain using X-ray crystallography and other common structural biology methods [1–3]. The technique uses comparative *in situ* labeling of solvent-accessible side chains by highly reactive hydroxyl radicals (•OH) in buffered aqueous solution under different assay conditions. In regions where a protein is folded or binds a partner, these •OH susceptible sites are inaccessible to solvent, and therefore protected from labeling. The •OH are generated by the ionization of water using high-flux-density X-rays. High-flux density is a key factor for XF-MS labeling because obtaining an adequate steady-state concentration of hydroxyl radical within a short irradiation time is necessary to minimize radiation-induced secondary damage and also to overcome various scavenging reactions that reduce the yield of labeled side chains.

This method, when first developed at the bending magnet beamline X28C at NSLS, required prolonged irradiation to yield detectable labeling on globular protein samples. The use of a focusing mirror revolutionized the XF-MS approach at X28C by delivering a high-flux density in milliseconds and brought unprecedented success to studies of megaDalton and membrane proteins complexes [4–7]. However, a major challenge in the introduction of sufficient hydroxyl radical dose without excessive exposure time or damage to complex protein samples persisted, despite the huge improvement in mass spectrometry resolution, sensitivity, and new analysis approaches over the past decade to target low-yield modification products. To address the challenge of inadequate flux density and extend the time scale of the method to the microsecond, we have used focused beam from a bending magnet X-ray source at the Advanced Light Source and developed a microfluidic sample handling procedure [8].

In this article, we will discuss the fundamentals of the XF-MS approach, recent methodological advancements, and recent applications illustrating the capabilities of bending magnet beamlines at the ALS to conduct XF-MS on the microsecond time scale, as well as the synergistic approach of combining footprinting with other synchrotron methods to solve ever more complex biological problems. We note that X-ray footprinting at the NSLS is transitioning to the NSLS II, and will resume operations in the coming year. During this transition period, a collaborative footprinting program is operating at the ALS footprinting beamline to support NSLS and NSLS II users.

The XF-MS Method

Low linear energy transfer radiation (LET), such as synchrotron X-rays in the range of 5–12 keV, interacts with water almost exclusively by the photoelectric effect and ionizes both bound and bulk water molecules, forming highly reactive hydroxyl radicals (•OH)[8]. The diffusible •OH undergoes productive reactions with proximal side chains and also counterproductive reactions with other •OH and buffer constituents in protein samples. Under aerobic conditions, the reactions with side chains result in covalent labeling such as hydroxylation, carbonylation, and di-oxidation, with specific signature mass adducts (+16, +14, +32 and +48 Da., etc.) [1]. The extent of labeling is quantified, and the site of labeling is identified by reverse-phase liquid chromatography coupled with high-resolution mass spectrometry following the standard protocol for bottom-up proteomics analysis. A progressive increase in the •OH dose results in a residue-specific dose response that, in turn, provides the side-chain-specific hydroxyl radical reactivity rate. The hydroxyl radical reactivity rate depends on both the intrinsic reactivity and the solvent accessibility of the residues.

Since XF-MS studies compare two or more states of proteins, the ratio of reactivity rates of the same residue from one state to another depends solely on the solvent accessibility difference between the two states. The radiometric information is interpreted in the context of existing high-resolution structures of one state and compared with that of an unknown state, or incorporated into molecular modeling strategies that provide information about protein or ligand docking and conformational changes [9, 10]. The counterproductive reaction pathways, which are discussed in detail in previous reviews, are a major limitation for the sensitivity of this method and are a major driver for the upgrades of beamline optics and hardware components in an XF-MS facility. While a significant increase in flux density can overcome •OH – •OH recombination, and the use of short irradiation times reduces protein damage, the use of non-scavenging buffer constituent requires strict quality control of samples before bringing them to the XF-MS facility [8]. In the

following section, we will review the advances undertaken at the ALS facility to counteract the loss of •OH dose in complex protein samples and increase the sensitivity of the method through upgrades in beamline components and other recent mass spectrometry approaches for data collection and analysis.

Beamline Configurations

XF-MS was originally developed at the monochromatic beamline X9A at the NSLS [11] and then transferred to a similar bending magnet but broadband X-ray beamline, X28C, which has been serving the user community since 2001 [4]. Installation of a palladium-coated toroidal focusing mirror produced a 10- to 20-fold increase in the effective dose compared to the unfocused source, and this increase in the flux density allowed users to successfully perform millisecond XF-MS on complex protein samples and *in vivo* systems. The proposed XFP beamline at NSLS II will utilize a three-pole wiggler source capable of delivering 10-fold higher flux density compared to X28C, and is due to be commissioned in 2016.

The XF-MS program at the Advanced Light Source (ALS) started in 2013 using beamlines 5.3.1 and 3.2.1. Beamline 5.3.1 is located on a bending magnet source and equipped with a platinum-coated toroidal focusing mirror suitable for focusing a white-light X-ray beam [8]. The broadband X-ray beam (1–13 keV) exits from the beryllium window of the beampipe under ultrahigh vacuum, with a flux of ~1×10^{16} photons/sec. The focused beam sizes can be set to deliver homogeneous flux density to match 100–535 mm ID microcapillary tubes, which are used to deliver samples using a syringe pump (Figure 1A). We have shown that, by using a microcapillary flow device and micron-sized beams, high-flux-density XF-MS can be carried out in the double-digit microsecond time scale (Figure 1B). Thus, a short pulse of high-flux-density photons produces adequate •OH concentration to overcome scavenging reactions, while preserving the structural integrity of complex protein assemblies. Beamline 3.2.1 is a white-light bending magnet beamline with similar characteristics to 5.3.1 but with no focusing mirror. This beamline is routinely used to study low molecular weight globular protein samples. The ALS has recently allowed beamline 3.3.1, which branches from the same bending magnet source as 3.2.1, to be commissioned for a dedicated XF-MS facility, which will be the one of highest-flux-density XF-MS facility in the United States in the coming years after installation of a focusing mirror and microcapillary sample handling hardware.

Recently, synchrotron protein footprinting studies were reported using several other low-flux-density synchrotron beamlines. However, these beamlines necessitated long irradiation times, resulting in secondary damage, which is time-dependent and results in specific structural perturbations. The experimental schemes for steady-state, time-dependent and temperature-dependent XF-MS methods are shown in Figure 2. We have introduced a new standard-flow liquid chromatography method with a high degree of chromatographic reproducibility and increased throughput for sample analysis. The SRM-based and MS/MS approaches developed by Case Western Reserve University researchers have improved the quality and sensitivity of the XF-MS approach for large protein complexes [2, 12]. Their recent introduction of the Protection Factor (PF) has shown that XF-MS can be used as a tool to quantitatively analyze protein topography.

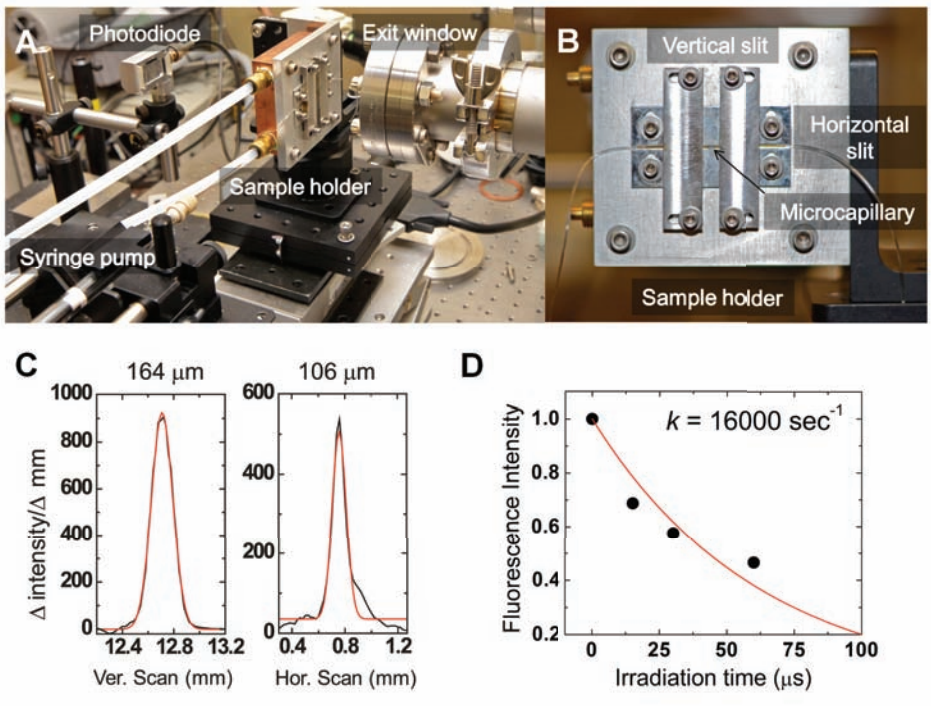

Figure 1: (A) The portable microcapillary flow set-up. The sample mount is assembled close to the ultra-high-vacuum beampipe that is capped with a Beryllium exit-window. (B) The horizontal slits on the sample mount hold the capillary horizontal to the beam. The photodiode shown in A is used for beam alignment. (C) The double derivative of the photodiode signal vs. vertical and horizontal scan of sample-mount estimates the FWHM of the beam on microcapillary. (D) The dose response plot of Alexa fluorophore, using the micron-size focused beam and 100 mm ID capillary tube on the sample mount. More than 70% Alexa fluorescence decay was observed within the double-digit microsecond irradiation time. The solid line represents a single exponential fit with a rate constant k = 16000 sec^{-1}.

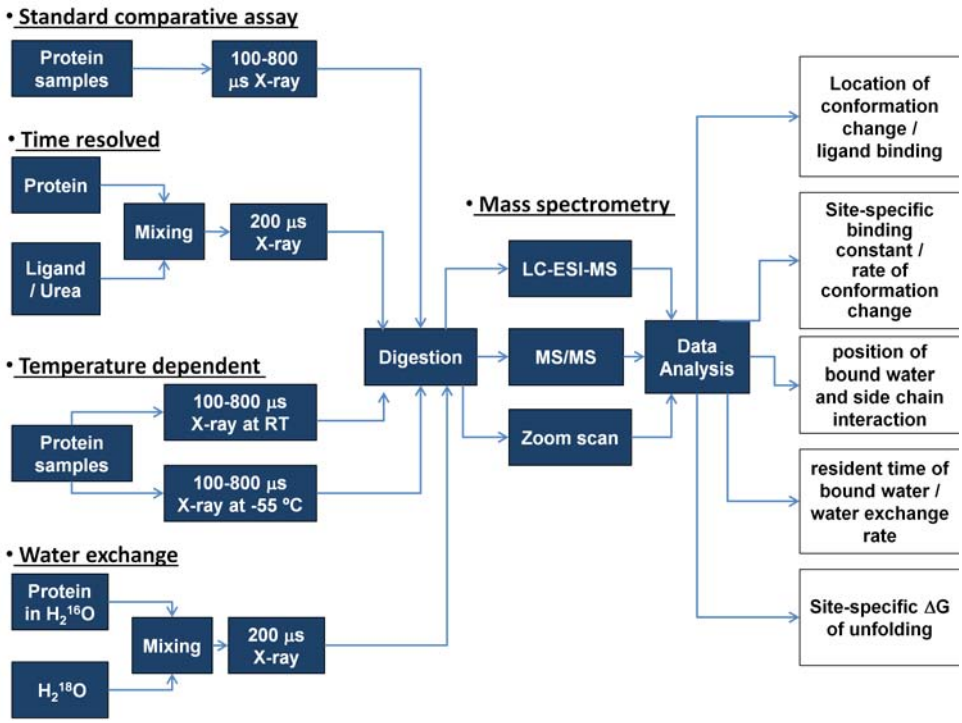

Figure 2: The schemes represent various types of X-ray radiolysis experiments, and the standard mass-spectrometry-based bottom-up proteomic analysis to measure structural information with a high degree of spatial and temporal resolution.

Comparison with Other Hydroxyl Radical Labeling Methods

Protein footprinting by hydroxyl radicals can be conducted without using a synchrotron. Chemical generation of hydroxyl radicals by oxidative Fenton chemistry is a simple lab-based method, for instance [13]. However, chemical production of hydroxyl radicals relies on the addition of reagents such as Fe-EDTA and H_2O_2 that can affect conformation or damage/unfold proteins, as well as remove essential metal ions necessary for protein function. The fast photochemical oxidation of the proteins (FPOP) approach uses dissociation of H_2O_2 by UV-LASER to generate a high concentration of •OH on the microsecond timescale [14]. However, the millimolar concentration H_2O_2 necessary can unfold proteins and/or perturb complex protein assemblies with metal-active centers. The electrospray-ionization (ESI) footprinting method uses electric discharge in the ESI component of the mass spectrometer to produce •OH, in which the protein is labeled in its semihydrated state in the presence of ammonium carbonate [13]. In contrast, the generation of •OH by ionizing radiation is very straightforward.

An alternate approach to X-ray radiolysis is electron beam radiolysis using a van de Graaff generator [15]. Unpublished data on cyt *c* and rhodopsin indicated that the electron pulse delivered is high enough to probe radiolytic modification in the sub-microseconds to microsecond time scale. However, unlike low LET ionizing radiation, the energy deposition by 2 MeV electrons can cause electron-induced protein damage that causes significant sample perturbation.

All of the •OH-based footprinting techniques have different advantages and disadvantages and, therefore, should be applied variously depending on the system under study. The unique advantages of synchrotron-based XF-MS include the following: First, the technique provides a straightforward way to vary the •OH dose from 5- to 20-fold by varying the flow rate of the sample across a fixed-size, continuous X-ray beam [8]. This simple approach is highly advantageous for generating dose-dependent data to determine precise hydroxyl radical reactivity rates for ratiometric comparisons between multiple states of complex biological samples [9, 16]. Second, *in situ* •OH generation has the advantage of allowing nearly any type of sample condition without deleterious effects from external reagents. Third, low LET X-rays can generate hydroxyl radicals by activating both bulk and protein-bond water, which can react directly with proximal side chains [17]. Protein-bound waters are often critical for protein structural stabilization, enzyme activity, ligand binding, and conformational change. Therefore, by probing the solvent accessibility of specific side chains adjacent to bound water, one can gather useful information on the dynamic role of bound water and internal H-bonding network for protein function.

Applications of the XF-MS Method

For the past several years, synchrotron-based footprinting studies have successfully provided significant insight into protein dymamics, structure of macromolecular assemblies, antibody eptiope mapping, and membrane receptor and ion channel proteins, many of which are of

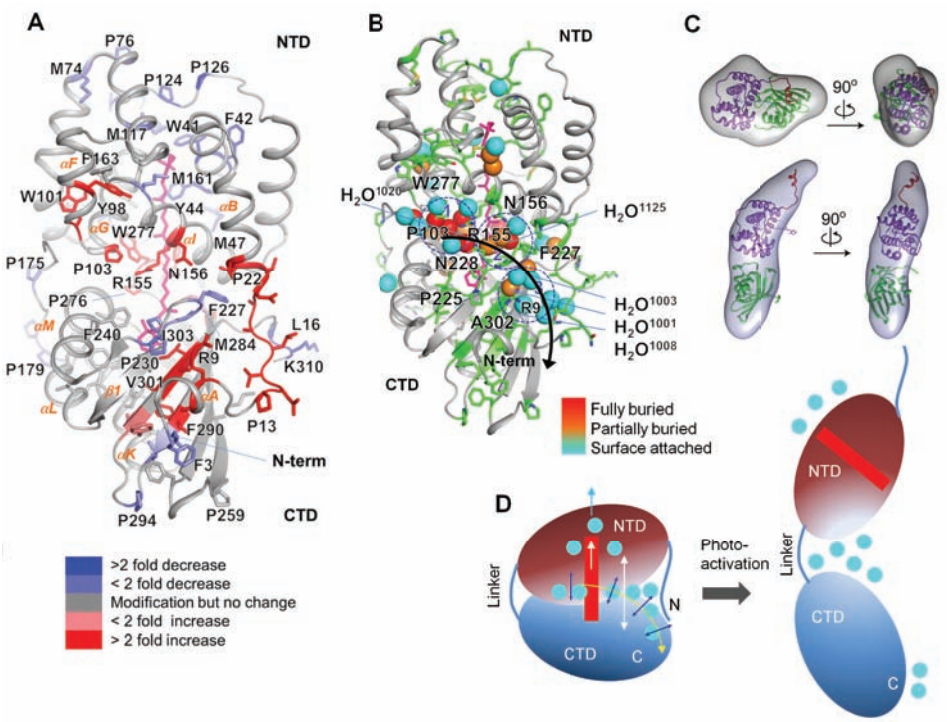

Figure 3: (A) Local structural changes in the Orange Carotenoid Protein (OCP) upon activation monitored by XF-MS. The modified residues are represented by sticks on the X-ray crystal structure of OCP^O (PDB ID code 3MG1). The carotenoid is shown in pink sticks. Color codes of the residues indicate the changes in solvent accessibility upon photoactivation (OCP^O to OCP^R). (B) Modified residues and the carotenoid are represented by green and pink sticks, respectively. The spheres represent conserved water molecules, and their color code indicates their depth from the surface of the OCP. Three major water clusters, at the interdomain interfaces, are marked by blue dashed lines. The black arrow indicates the proposed signal propagation pathway from the carotenoid through the water-side-chain H-bonding network to the protein surface that facilitates carotenoid shift, dissociation of NTD-CTD, and detachment of the N-terminal helix from CTD. (C) Ab-initio bead reconstructions (gray volume) using GASBOR are shown for OCP^O and OCP^R. Similar results were obtained using other bead modeling algorithms. A single subunit of OCP^O from the crystal structure is docked into the volume envelope with the far N-terminal helix (red), N-terminal domain (NTD; purple), and C-terminal domain (CTD; green) (PDB ID code 3MG1). The two domains of OCP along with the N-terminal helix were modeled to approximate the volume envelope of OCP^R, showing dissociation of NTD and CTD. (D) Schematic of the OCP^O and OCP^R showing regions with the largest conformational rearrangement associated with the change in H-bonding network and water rearrangements.

therapeutic interest for health science research. Until now, the application of XF-MS to environmental research and bioenergy solutions has been limited, but we can envision research using XF-MS on proteins and enzymes that are involved in bioenergy solutions, biosequestration, and bioremediation. The ALS is an ideal location for just such programs, as several large-scale efforts in these areas are housed at institutions a short distance away. For instance, the Joint BioEnergy Institute (JBEI) is dedicated to programs in biofuel synthesis using bioengineered proteins for plant growth and deconstruction of plant material. The Joint Genome Institute (JGI) pursues programs in characterizing proteins that contribute to carbon cycling. The Biosciences Area at Berkeley Lab brings together researchers at both the lab and on the UC Berkeley campus to study protein systems related to carbon sequestration, bioremediation, and energy-harvesting systems. As an example of one such successful collaboration with researchers at the JGI, we have demonstrated the use of XF-MS to study a photosynthetic protein component relevant for understanding and bioengineering of artificial photosynthetic systems [18, 19]. Photoprotective mechanisms are of fundamental importance for the survival of the photosynthetic organism. In cyanobacteria, the orange carotenoid protein (OCP), when activated by intense blue light, forms OCPR, which binds to the light-harvesting antenna and triggers the dissipation of excess captured light energy. X-ray crystal structures of inactivate OCP (OCPO) and the N-terminal part of OCPR (RCP) are available. The comparison between these two structures shows that, during photoactivation, the carotenoid moves by about 12 Å inside the N-terminal half of OCP. A comparative XF-MS study of OCPO and RCP showed protection of specific residues at the N-terminal domain (NTD) and supported carotenoid translocation in a solution similar to that in the RCP crystal structure. Since RCP was only a part of OCPR, uncertainty about structural changes in the full-length OCPR persisted. However, a hybrid approach comprised of XF-MS, SAXS, and hydrogen deuterium exchange mass spectrometry (HDX-MS) provided mechanistic details of the conformational changes for the photoactivation of full-length OCPO to OCPR. While the SAXS data showed that light activa-

tion was accompanied by structural changes that reflected dissociation of the NTD and C-terminal domain (CTD), representing a globular to elongated global conformational change, HDX-MS indicated that the majority of the secondary structure was unaltered during this process. XF-MS, however, yielded detailed residue-specific solvent accessibility changes that supported both domain dissociation and carotenoid translocation in the full-length protein. In addition, XF-MS identified several functionally important residues involved in a H-bonding network with bound as well as conserved water molecules at the major and minor interfaces of the NTD and CTD. Overall, the hybrid approach suggested that the carotenoid translocation induced changes in the water-protein network that transmitted the signal to the protein surface (Figure 3). This work provided the detailed molecular mechanism underlying the initiation of cyanobacterial photoprotection. Further studies on the interaction of OCP with the phycobilisome [20] and the fluorescence recovery protein [21] will provide complete details of the photoprotection cycle in photosynthetic systems. Other ongoing work related to bioenergy is in the area of footprinting of shell components of bacterial microsomes, with applications for sequestering and controlling enzymes involved in carbon cycling. A further application with wide-reaching potential is in the footprinting of proteins *in vivo* in live cells. Preliminary experiments in this area have been conducted on several *E. coli* systems, with promising results. In addition, high-throughput and fast-mixing methods are under development to increase the capabilities of the X-ray footprinting method.

Synergy of XF-MS with Other Synchrotron Methods

The local changes in solvent accessibility deduced from XF-MS are complemented effectively with high-resolution structures obtained from X-ray crystallography, as well as with low-resolution global structural methods such as small angle scattering and CryoEM techniques to provide a comprehensive picture of the structure-function relationship. Specifically, crystallographic data of a non-functional or non-bound state has often enriched footprinting interpretations of the functional or bound state [3]. The method of XF-MS can be used to directly pinpoint both positional and dynamical aspects of water-protein interactions and, recently, it has opened a path forward for understanding the function or activation of many important proteins [17]. The example highlighted earlier showed how XF-MS was used to interpret protein conformational changes associated with the dynamics of proximally bound water, which are determined from the available crystal structures of the native state [19].

The combination of local structural information provided by XF-MS with SAXS has already proven valuable for understanding protein structure and dynamics; for example, analyses of SAXS data were consistent with formation of an intermediate in the Ca^{2+} activation of gelsolin as suggested by XF-MS; the combined picture defined the structure of the intermediate Ca^{2+} bound state [22, 23]. More recently, SAXS, SANS, and XF-MS were combined to provide a molecular model of the core of bacterial segrosome assembly, highlighting the value of obtaining both global and local measurements and integrating the data with available crystallographic information in a comprehensive modeling framework [24]. The resolution of SAXS data does not permit evaluation of bound water dynamics; however, in a combination with time-resolved XF-MS, a valuable understanding of conformational dynamics can be obtained since both techniques use similar sample handling conditions in solution, as shown in the current studies on OCP [19].

Outcome of Workshops

The XF-MS program at the ALS was initiated in part to support the users who need access to a footprinting facility while the new beamline at the NSLS-II (XFP, on BM-17) is constructed. We have been organizing XF-MS workshops for past two years. The XF workshop at the 2014 ALS Users Meeting titled "X-ray Footprinting at the ALS: New Opportunities in Structural Biology" brought together a group of researchers from around the country to discuss the capabilities of footprinting, as well as recent exciting advances in XF-MS data analysis and areas of protein-protein interactions, ligand binding, and bound water interactions and dynamics. The workshop covered experimental techniques, tutorials on data analysis and new software available for the technique, as well as hybrid approaches (SAXS and XF) [12, 25, 26]. The second half covered recent science highlights, including results on ribosome assembly in live cells [27], the conformational changes governing photoprotection in cyanobacteria [18], analysis of amyloid fibrils [28], internal water interactions in membrane proteins [9], determining antibody conformations [29], and HIV ENV glycoprotein activation [30]. The workshop concluded with a talk describing the capabilities of the new XFP beamline currently under construction at the NSLS-II, and a tour of the ALS beamlines now supporting the XF community. The workshop at the 2015 ALS Users Meeting titled "Hybrid Methods for Integrative Structural Biology" was a joint workshop between the ALS and the Stanford Synchrotron Radiation Laboratory and covered a wide range of methods for structural interrogation of biological molecules, including well-established methods such as macromolecular crystallography and cryo-electron microscopy, as well as relatively new methods such as X-ray footprinting. Since many biological systems cannot be understood via one structural or dynamics method alone, several invited talks were chosen to highlight a combination of methods necessary to gain insight into an important biological problem.

Concluding Remarks

XF-MS is now established as robust method to determine both global and local structure, and can be used synergistically with other high-resolution structural techniques. XF-MS offers unique information on protein-water interactions and, as such, is a highly complementary technique to more well-known structural methods. Currently, dedicated XF-MS beamlines are under development at both the ALS and NSLS II. These beamlines are designed for fully automated sample handling, microsecond irradiation timescales, and time-resolved experiments. Advancement in XF-MS allows for the real possibility of delineating detailed molecular mechanisms and ligand binding in protein structure and function. ■

References

1. G. Xu and M.R. Chance, *Chemical Reviews* **107**, 3514–3543 (2007).
2. J.G. Kiselar and M.R. Chance, *J Mass Spectrom* **45**, 1373–1382 (2010).
3. V.N. Bavro et al., *Biochem Soc Trans* **43**, 983–994 (2015).
4. S. Gupta et al., *J Synchrotron Radiat* **14**, 233–243 (2007).
5. M.R. Sullivan et al., *The Review of Scientific Instruments* **79**, 025101 (2008).
6. T.E. Angel et al., *Proceedings of the National Academy of Sciences of the United States of America* **106**, 14367–14372 (2009).
7. J. Bohon et al., *Structure* **16**, 1157–1165 (2008).
8. S. Gupta et al., *J Synchrotron Radiat* **21**, 690–699 (2014).
9. S. Gupta et al., *Nature* **512**, 101–104 (2014).
10. J.K. Kamal and M.R. Chance, *Protein Sci* **17**, 79–94 (2008).
11. C.Y. Ralston et al., *Methods in Enzymology* **317**, 353–368 (2000).
12. P. Kaur et al., *Mol Cell Proteomics* **14**, 1159–1168 (2015).
13. S.D. Maleknia and K.M. Downard, *Rapid Communications in Mass Spectrometry: RCM* **26**, 2311–2318 (2012).
14. D.M. Hambly and M.L. Gross, *Journal of the American Society for Mass Spectrometry* **16**, 2057–2063 (2005).
15. C. Watson et al., *Analytical Chemistry* **81**, 2496–2505 (2009).
16. S. Gupta et al., *Structure July* (2010).
17. S. Gupta et al., *Proceedings of the National Academy of Sciences of the United States of America* **109**, 14882–14887 (2012).
18. R.L. Leverenz et al., *Science* **348**, 1463–1466 (2015).
19. S. Gupta et al., *Proceedings of the National Academy of Sciences of the United States of America* **112**, E5567–5574 (2015).
20. D. Kirilovsky and C.A. Kerfeld, *Photochem Photobiol Sci* **12**, 1135–1143 (2013).
21. M. Sutter et al., *Proc Natl Acad Sci U S A* **110**, 10022–10027 (2013).
22. J.G. Kiselar et al., *Proc Natl Acad Sci U S A* **100**, 3942–3947 (2003).
23. M.S. Ashish Paine et al., *J Biol Chem* **282**, 25884–25892 (2007).
24. B.N. Chaudhuri et al., *Biochemistry* (2010).
25. W. Huang et al., *Adv Mater* **26**, 7902–7910 (2014).
27. S.F. Clatterbuck Soper, *Mol Cell* **52**, 506–516 (2013).
28. A.L. Klinger et al., *Biochemistry* **53**, 7724–7734 (2014).
29. G. Deperalta et al., *MAbs* **5**, 86–101 (2013).
30. M. Guttman et al., *Structure* **22**, 974–984 (2014).